Bistatic Synthetic Aperture Imaging of Proud and Buried Targets From an AUV

Kevin D. LePage and Henrik Schmidt

***Abstract*—The use of autonomous underwater vehicles (AUVs) for the detection of buried mines is an area of current interest to the Mine CounterMeasures (MCM) community. AUVs offer the advantages of lower cost, stealth, reduced operator risk, and potentially improved coverage rates over more traditional mine hunters. However, AUVs also come with their own set of difficulties, including significant error in navigation and low communication rates with the mother platform and each other. In the case of bistatic detection scenarios, AUVs will therefore have difficulty knowing where exactly in space they are and the trigger time of sources on other platforms, be they ships or other AUVs. However, the potential improvement in detection and coverage rates offered by bistatic sonar concepts makes resolution of these issues a high priority. In this paper, the problems of inaccurate navigation and source timing information are addressed for the Generic Oceanographic Array Technology data set. In this experiment, conducted off Marciana Marina during June 1998, a MIT AUV with a SACLANTCEN acoustic array and acquisition system was used together with a TOPAS parametric sonar to explore issues of buried target detection using AUVs. In this paper, solutions to the navigation and timing problems are proposed which enable the effective use of bistatic synthetic aperture sonar (SAS) concepts for the detection of buried objects in the mid-frequency regime of 2–20 kHz.**

***Index Terms*—Buried object detection, multistatic scattering, synthetic aperture sonar, underwater vehicles.**

I. Introduction

In June of 1998, a joint MIT/SACLANTCEN experiment called Generic Oceanographic Array Technology (GOATS'98) was conducted off Marciana Marina on the island of Elba in the Tyrrhenian Sea in shallow water, for the purpose of evaluating the detection of mine-like objects buried in the seafloor [1]. A MIT Odyssey II AUV equipped with a SACLANTCEN acoustic nose array and acquisition system was used to survey the scattering from a target field excited by the Centre's highly directional TOPAS parametric array at various grazing angles ranging from above to below critical angle. Subcritical detection of buried objects is an important goal of advanced mine hunting sonar concepts, but the extremely low insonification levels on buried objects at incident angles below the critical angle of the sediment-water interface imply that significant array gains are required to make object detection feasible. The conventional approach to obtaining the required gain is to explore synthetic aperture sonar (SAS) concepts [2]. The GOATS'98 data set, with inherently inaccurate navigation data from a long baseline (LBL) navigation system, bistatic source-receiver geometries and a lack of TOPAS trigger times due to communication limitations between the AUV and the TOPAS, places new demands on SAS concepts. In this paper, these limitations are addressed and subcritical detection of buried objects on a bistatic synthetic aperture collected by an AUV in the 2–20-kHz frequency band is demonstrated.

Manuscript received April 2, 2001; revised July 29, 2001. The work of H. Schmidt was supported by the Office of Naval Research.

K. D. LePage is with the SACLANT Undersea Research Centre, La Spezia 19138, Italy (e-mail: lepage@saclantc.nato.int).

H. Schmidt is MIT Professor of Ocean Engineering, Cambridge, MA 02139 USA (e-mail: henrik@keel.mit.edu).

Publisher Item Identifier S 0364-9059(02)06360-4.

II. Experimental Description

The experimental geometry of GOATS'98 is shown in Fig. 1, where the target field, consisting of three 1-m inner diameter, 3-cm thick water-filled steel spheres S1, S2, and S3, with center burial depths of 1, 0.5, and 0 m are shown being insonified by a TOPAS source generating a highly directional beam in the secondary frequency band of 2–20 kHz. These spheres had lifting lugs consisting of bar with a 2×5 cm cross section bent to the shape of a triangle of 5.5-cm height and 22-cm width attached to their tops but no other attached buoys or other objects. At the wavelengths considered in this paper, greater than 10 cm, the spheres can be considered acoustically clean. The depth of the water over the target field was 13.5 m and a 128-element horizontal line array (HLA) was deployed over S2 in the position indicated by the green line. Data from this HLA are not analyzed in this paper. The TOPAS source itself was mounted on a 10-m tall tower which could be moved along a horizontal rail lying on the seafloor. The average depth of the TOPAS rail was 14.3 m. Taking into account the slight difference between the bottom depth at the TOPAS and at the target field, this tower and rail arrangement allowed the angle of incidence of the TOPAS beam on the seafloor above the flush buried sphere S2 to be adjusted between 16.2° and 34.6° [1]. This range of incident angles included the important subcritical grazing angles below 22.9°, as the bottom in the Marciana Marina area is sandy with an average near sediment-water interface sound speed of approximately 1650 m/s in the frequency band of interest [3]. It is important to note that the seabed in the vicinity of the targets was relatively flat and free of ripples, due to the disturbance and smoothing of the sand associated with the placement and burial of the targets and the lack of subsequent storm activity [1].

The MIT Odyssey II AUV was programmed to swim missions over the target field while various targets were directly insonified by the TOPAS at various grazing angles. The vehicle transited the target field at an average height of approximately 7.5 m and at an average speed of approximately 1 m/s. In this paper, we confine our attention to the data set x9814501, where

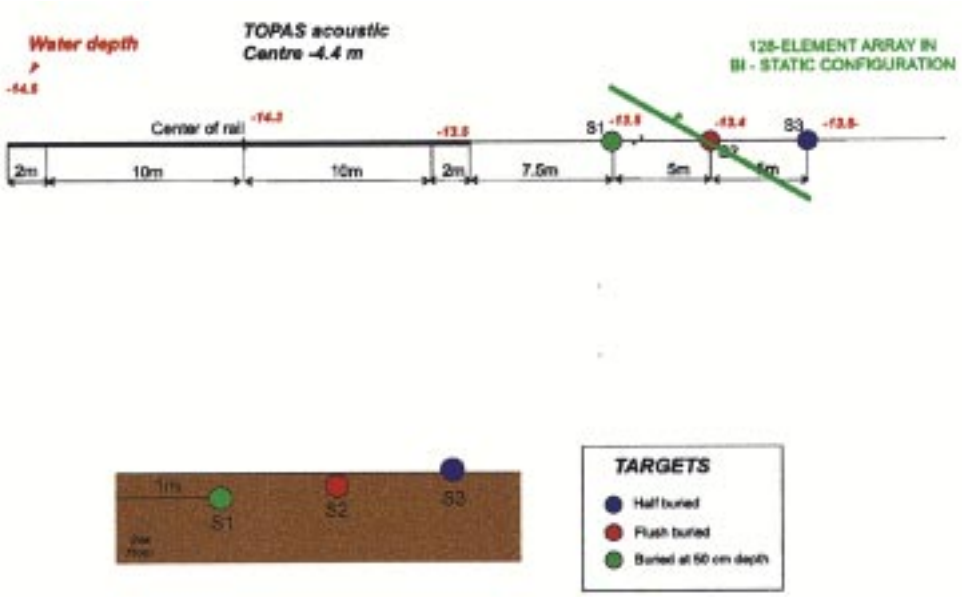

Fig. 1. The experimental configuration for GOATS'98 showing the 10-m tall TOPAS tower at a 10-m rail position which illuminates the target field of buried spheres. The TOPAS position for the data collected during experiment x9 814 501 is 5 m further to the left, from which point the flush buried sphere S2 is insonified below critical angle at an angle of 17.0°. The data analyzed for experiment x9 814 601 were collected when the source was 2.5 m further to the right, from which point S2 was insonified at 22.5°.

the TOPAS tower was at a 5-m position along the rail and was aimed at the proud target S3 at a 14.8° grazing angle and to the data set x9814601, where the TOPAS tower was at a 12.5-m position along the rail and was aimed at the flush buried target S2 at a 22.5° grazing angle. In the first experiment, the TOPAS tower was 34.5 m from the proud sphere and with its 4° vertical and 9° horizontal beampattern [5] it insonified a patch centered on S3 which extended roughly 9.2 m in range and 5.5 m laterally. In this geometry, the flush buried sphere S2 was insonified at a grazing angle of 17.0° and because of the size of the insonified patch, it received adequate power to be detected. However, because S2 was illuminated at an angle roughly 5° below the critical angle, the scattered returns measured from this target are significantly smaller than those measured from the proud sphere S3. In the second experiment, both S2 and the deeply buried sphere S1 were insonified at or above the critical angle, making their detection significantly easier.

Since the Odyssey AUV was operating without time synchronization with the TOPAS system, it was decided to trigger the TOPAS off the AUV's navigation interrogation pulse. Every ten seconds, the vehicle would interrogate the LBL system with a 9-kHz transmission. The LBL network, which consisted of six buoys with transponders operating in the 8–10.5-kHz range, would then respond and the vehicle computer would use the round trip travel times to update its navigational estimate. The TOPAS would also detect the AUV's interrogating pulse and after waiting 2 s for the reverberation from the transponders to die out, would commence to broadcast 8-kHz Ricker [4], [5] waveforms at a source level of 201 dB re 1 μPa every 300 ms. At the same time the interrogating pulse was sent, the acquisition system on the AUV would begin to collect a 10-s long data file (called a "ping") off an eight-element horizontal line array of hydrophones which was deployed off the nose of the vehicle as illustrated in Fig. 2. This array was designed to receive the scattered field caused by the illumination of the target field by the TOPAS and has a design frequency of 7.5 kHz and a sample rate of 50 kHz. Since the total field interrogated by the AUV nose array had a large dynamic range, the acquisition system, which was only a 16-b system with 84–90 dB of dynamic range, was designed with 16 channels so that the field could be collected at two gain settings 40 dB apart.

Estimates of the vehicle trajectory during experiment x9 814 501 are illustrated in Fig. 3. The accuracy of the vehicle navigation was quite poor from an acoustic point of view. The inexact measurement of the LBL transponder locations, the unknown sound-speed field between the transponders and the AUV, the strong multipath arrival structure of the shallow water environment, and the state of the art in the AUV navigation filters together placed very coarse limits of ± 1 m on the vehicle location. In addition, significant biases were seen in the navigation for south traveling legs which implied unresolved problems with the navigation software [1]. Thus, while the acoustic measurements made on the swordfish array were of generally good quality, with sufficient reverberation-to-noise ratio (RNR) to image targets, the coherent combination of these data over successive TOPAS transmissions to create a synthetic aperture, represents a challenge. In addition, the exact time of the TOPAS transmissions is unknown, due both to the fact that the vehicle acquisition system was unsynchronized to the TOPAS system and to the fact that the standard deviation of the TOPAS firing time itself was approximately 10 ms. Thus, the straightforward application of conventional monostatic synthetic aperture concepts was clearly not possible and the problems of inaccurate vehicle position and unknown source trigger time and location need to be circumvented in order to demonstrate SAS concepts for this data set.

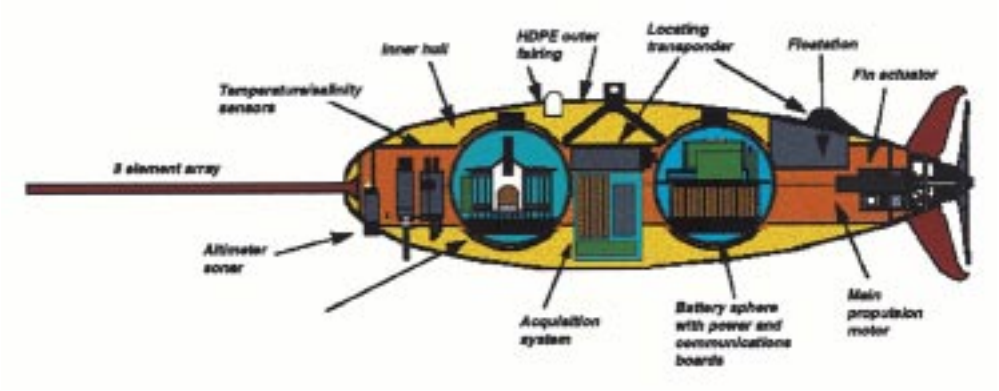

Fig. 2. A diagram of the MIT Odyssey AUV showing the 0.7 m-long eight-element "swordfish" array deployed off the bow and the 50-kHz-16-channel-dual-gain acquisition system amidships. The element spacing of the array is 10 cm.

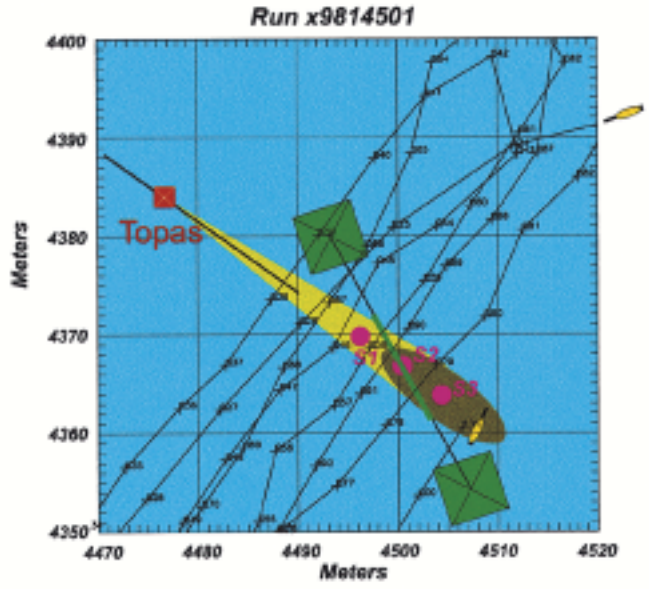

Fig. 3. The AUV trajectory during GOATS'98 experiment x9 814 501. Bistatic scattering from targets S2 and S3 is measured on the AUV as it swims back and forth over the target field. The green boxes indicate the towers from which the 128 element HLA, indicated by the green line, was deployed. Data from ping 25 is processed in this paper.

III. Experimental Results

A spectrogram of a typical "ping" collected on the AUV nose array is illustrated in Fig. 4. The data analyzed in this paper were all collected at the 40-dB gain setting on the AUV acquisition system in order to have good headroom over bit noise on the scattering from buried targets and the reverberation from the target field. The AUV acquisition system began recording 10 s of time series off the nose array after instructing the AUV navigation system to begin an LBL interrogation sequence. The clipped returns from the six LBL transponders operating at 500-Hz intervals between 8 and 10.5 kHz are seen at times between 0.3 and 0.6 s at the left of the spectrogram. The TOPAS detected the LBL interrogation cycle and after waiting 2 s for reverberation from the LBL cycle to die down, began sending 8-kHz Ricker pulses every 300 ms. On average, 24 TOPAS transmissions are recorded during each 10-s AUV acquisition cycle. These 10-s data files are called "pings". The individual TOPAS transmissions are visible as the vertical stripes on the spectrogram. During these transmissions, the AUV was traveling at an average speed of approximately 1 m/s or 2 kts. The rate of the TOPAS transmissions, the vehicle velocity, and the length of the swordfish array together determine that only roughly the front three of the eight elements of this array collect new information about the field scattered from the target area for each consecutive transmission. The fact that there is significant array overlap between successive transmissions means that autofocusing concepts from traditional SAS [6]–[8] may be used to help resolve difficulties associated with navigational uncertainty and trigger timing.

Although as illustrated in Fig. 4, the TOPAS fires roughly every 300 ms, the trigger times are quite imprecisely known, with a standard deviation on the order of 10 ms due to the design of the TOPAS trigger. Thus, when snippets of data are extracted and stacked, there is an evident lack of synchronization of the arrivals associated with the source and the various targets. For traditional monostatic MCM sonars, the returns scattered from the target field would be known in absolute time from the source trigger time, since the source trigger is readily available on a monostatic platform. For bistatic situations such as in the GOATS'98 data set, the source trigger time and the total absolute travel time from the source to the target field and back is only approximately known. To give a better feel for the distinguishing characteristics of the data, 100 consecutive 65-ms snippets of time series from the first element of the nose array from pings 23 through 27 (the approximate physical locations of the "pings" for experiment x9 814 501 are shown in Fig. 3) have been extracted and aligned by the time of the first scattered return from S3 (37 ms). The results, which contain the TOPAS direct arrivals and target scattered returns, are shown in Fig. 5. The strongest feature is the direct scattered return from the proud sphere S3 on which the data have been aligned. Right behind this return is an almost equally strong surface multiple of the same arrival. These two returns have a signal-to-reverberation ratio (SRR) of about 15 dB. Two further surface-bottom multiples are faintly visible to the far right at times between 47 and 57 ms. The fairly strong return seen for ping 25–27 at a time of 46 ms is believed to be a scattered return from the HLA shown in Fig. 1. The three fainter returns to the far left, arriving at arbitrary times between 17 and 25 ms,

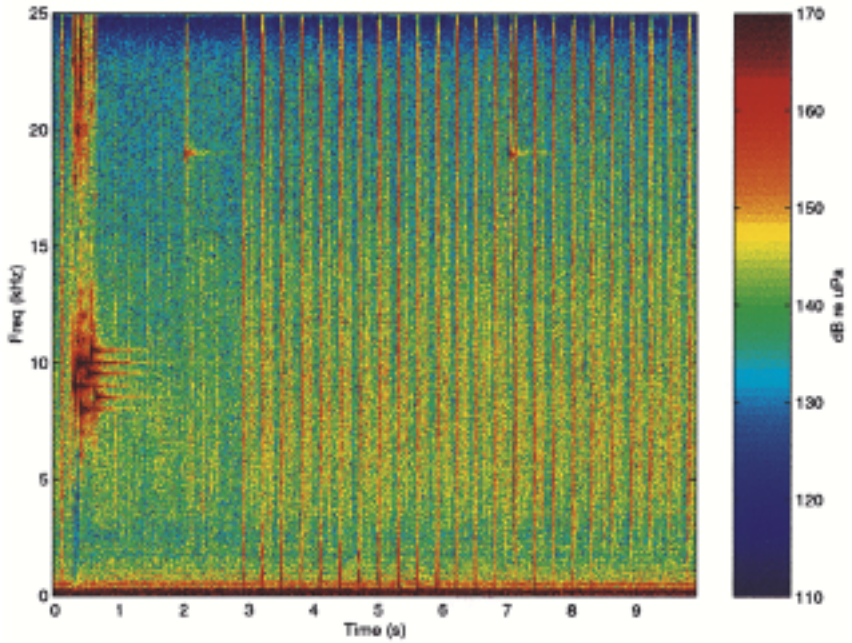

Fig. 4. Spectrogram of ping 25 of the AUV data acquisition system from experiment x9 814 501 shows the LBL interrogation pulses followed 2 s later by 24 TOPAS transmissions on the proud target S3 at 300-ms intervals.

are the direct arrival and the first bottom and surface multiple of the direct blast from the TOPAS. The reason that the amplitude of the source arrivals is smaller than the scattered returns from S3 is because the AUV is out of the main transmission beam of the TOPAS.

The scattered returns from the flush buried sphere S2 are just visible in the data between the times of 32 and 35 ms. These returns have an SRR of approximately 6 dB, although it can vary from 0 to 10 dB. Unlike the return from the proud sphere S3, there are clearly two returns associated with the target itself. It is hypothesized that the first of these returns is not a specular return from the flush buried sphere, but rather the first round trip of the S_o membrane wave and that the second return, which comes approximately 0.5 ms later, is the first antisymmetric bending wave $A_{o\_}$ multipath [9], [10]. In fact, close inspection of Fig. 5 shows that a third, very faint arrival associated with S2 arrives another 0.5 ms earlier than the first of the two larger returns. It is this return which we identify as the specular return from S2. The amplitude of these two returns from S2 are significantly lower than those of the single strong return from S3 and are not too far above the reverberation background of the bottom patch insonified along with S3. In Fig. 6, all eight channels of the nose array for 20 consecutive TOPAS transmissions from ping 25 are shown enlarged to better appreciate the details of the data. In this case, the time series have been aligned along the axis of the direct blast from the TOPAS. All eight time series from the nose array on the AUV are shown for each ping. The relative amplitude of the S2 and S3 returns may be appreciated from this figure. In addition, the increased reverberation from the insonified patch may be observed in the individual time series to begin at the arbitrary time of roughly 27 ms.

In order to estimate the vehicle velocity a correlation log procedure [11] was applied to the part of the time series shown in Fig. 6 which was between the times of 27 and 36 ms. The results are illustrated in Fig. 7, where the peak cross correlation value between successive transmissions received on the physical aperture is shown averaged over the front four array elements of the nth transmission. It is seen that the average correlation lag between the n and $n+1$ transmissions is roughly 4 spatial elements (1 element corresponding to no motion), while between the nth and $n+m$ transmissions it is $N(m-1)+1+(lag-1)m$ where $N=8$ is the number of elements in the physical aperture. For $m=2$, this gives a peak spatial correlation at 15 elements, which is also seen in Fig. 7. For m greater than 2, there is no correlation because the physical aperture no longer overlaps its previous position after two subsequent transmissions. This behavior is explained schematically in Fig. 8. The peak correlation (ρ^2) values themselves lie between 0.7 and 0.9, corresponding to RNR between roughly 4 and 10 dB. A correlation value of 0.5 corresponds to a RNR of 0 dB.

In Fig. 9, the velocity estimate of the vehicle and the lag of the maximum correlation in μs are shown in a semilog format. The abscissa is the total time occupied by the 20 transmissions and the ordinate is either the vehicle speed in knots (shown in blue), or the lag time (in red). These results show that the average maximum correlation lag of three elements or 3×0.1 m/300 ms $\equiv$ 1 m/s corresponds to vehicle speeds between 1.8 and 2.3 kts and that the maximum correlation occurs at time less than 0.1 ms from times obtained by manual alignment of the time series to the direct TOPAS arrival as shown in Fig. 6.

Under the assumption that the AUV follows a straight trajectory during a single 10-s duration acquisition cycle, it may be hypothesized that a useful synthetic aperture of the scattered field measured during a single acquisition cycle may be constructed by simply appending the successive transmissions at the spatial point of maximum correlation shifted in time by the appropriate correlation lag. Thus, referring again to Fig. 8, only

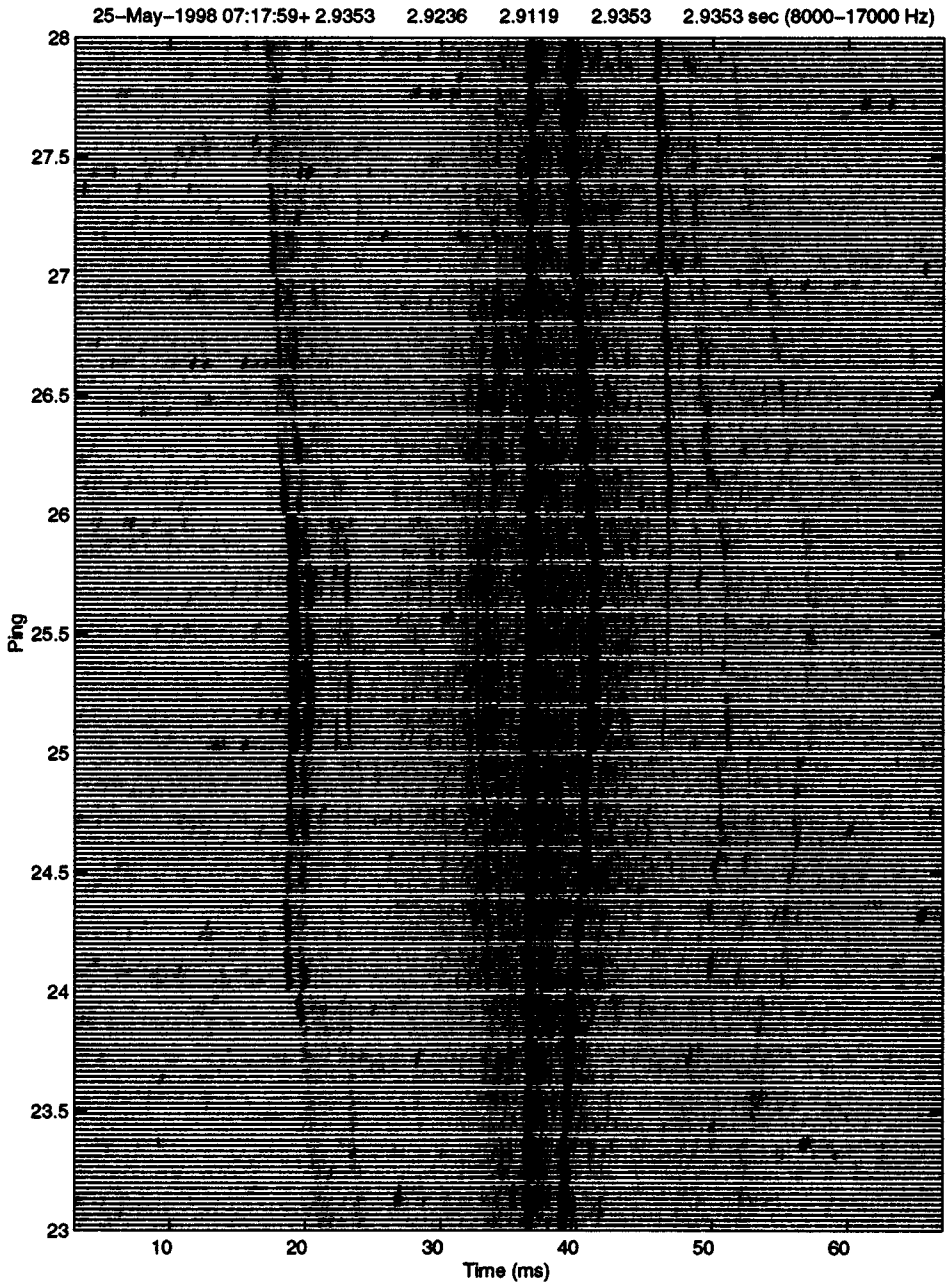

Fig. 5. The time-series data from pings 23 through 27 are shown in the 8–17-kHz band aligned by the time of arrival of the first scattered return from S3 (37 ms). The first surface multiple of the S3 return is clearly visible at times between 39 and 41 ms. The direct TOPAS arrivals and the first surface and bottom multiples are visible at times between 17 and 23 ms. Two scattered returns from the flush buried sphere S2 are also faintly visible at arbitrary times between approximately 32 and 35 ms.

the time series of elements 1 through 3 from the second transmission are appended onto the vector time series from the first transmission. Similarly, only the first three elements of the third transmission are appended onto the growing synthetic aperture consisting of all eight elements from the first transmission and the first three lements from the second. On each subsequent transmission, the best spatial correlation lag is determined by averaging the maximum spatial correlation found for the first four elements of the synthetic aperture and the new time series are appended at the corresponding time lag of the maximum correlation. The result of this process is illustrated in Fig. 10. Here, the two arrivals from S2 and the first scattered return from S3 are both clearly visible. The size of the synthetic aperture is 6.3 m or roughly nine times the length of the physical aperture of the array. The curvature of the S2 and S3 arrivals also clearly indicate that these targets have been received in the nearfield of the synthetic aperture.

The hypothesis that the AUV trajectory is a straight line during the 10-s acquisition cycle can be tested by attempting to fit the hypothetical arrival times on a straight trajectory to the measured arrival times from a target of opportunity. In the case of experiment x9814501, the insonification of S3 always provides a clear scatterer of opportunity. The results of the fit of the arrival times of S3 to a straight trajectory hypothesis

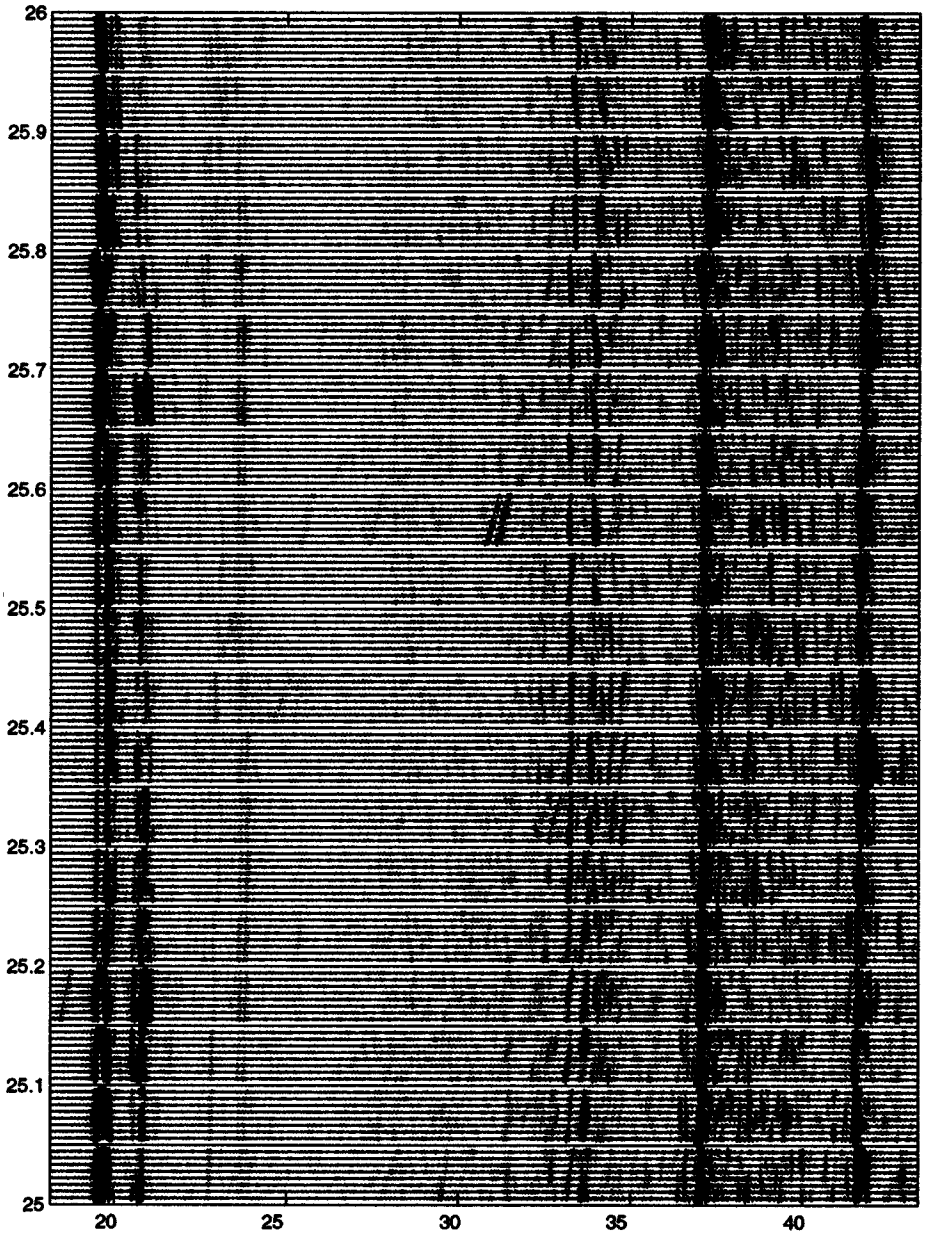

Fig. 6. Closeup of the bandpassed scattered field received on all eight elements of the nose array of the AUV for 20 TOPAS transmissions in ping 25 of experiment x9 814 501. Here, the large S3 arrival at 47 ms and the two S2 arrivals at 43.5 and 44 ms are clearly visible. Moveout of the arrivals on the individual eight-element arrays is minimal, indicating that the scatterers are observed near broadside during this ping. Also, clearly visible is the scattering from the rough sand in the insonified footprint of the TOPAS, beginning around 37 ms.

are illustrated in Fig. 11. The fit based on a straight AUV trajectory at a constant depth is very good and carries the added benefit that the standoff distance x from the AUV to the target (here $x = 8.8$ m assuming a background sound speed of $c_o = 1520$ m/s) is a byproduct of the fit procedure. The proximity of the scatterer to the AUV trajectory is determined by the curvature of the arrival structure at the point of closest approach. Under the hypothesis of straight travel, it is seen that the problem of the unsynchronized AUV data may be largely overcome, with the additional benefit that in the case of nearfield scatterers an estimate of the vehicle standoff distance may be obtained and evaluated for consistency with navigational data obtained from the LBL network.

IV. Bistatic Synthetic Aperture Processing

The autofocused data shown in Fig. 10 may be processed coherently over the near-field synthetic aperture by a simple bistatic SAS algorithm. In arbitrary time coordinates, the time of arrival of the return from a point scatterer of opportunity (S3 in the processing described in this paper) from a bistatic source a distance R from this scatterer is (see Fig. 12)

$$T_{S3} = \frac{R}{c_o} + \sqrt{x_o^2 + (y - y_o)^2 + \frac{z_o^2}{c_o}} + T_o \qquad (1)$$

where T_o is the arbitrary offset time, x_o is the horizontal point of closest approach of the linear AUV trajectory to S3, z_o is the

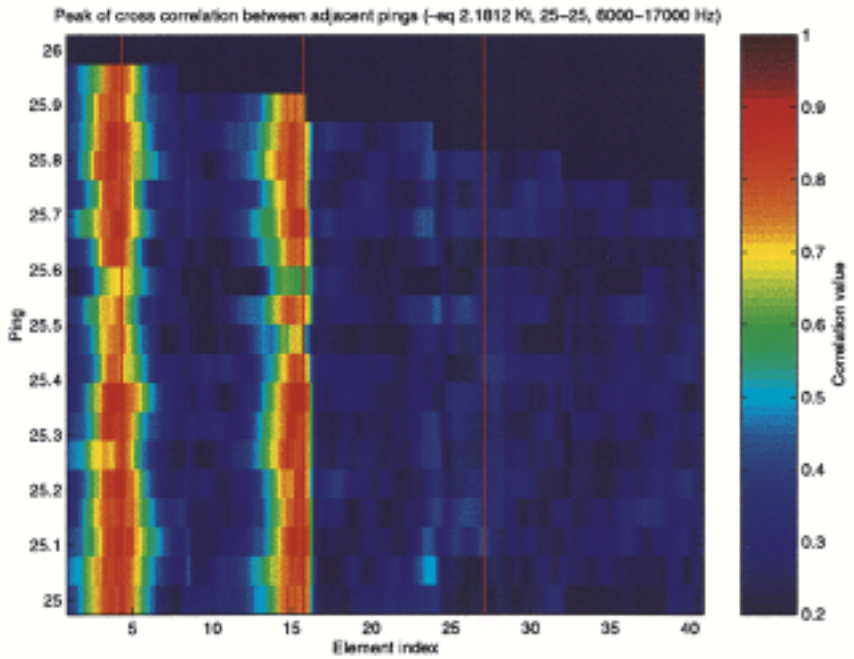

Fig. 7. The maximum inter-transmission correlation coefficient vs physical element index. The far left corresponds to the correlation coefficient between the first element of physical aperture for the n and $n+1$ transmissions, corresponding to no array displacement. Instead the largest coefficient is seen between the first element of the nth transmission and the fourth element of the $n+1$ transmission, corresponding to physical displacement of three elements between TOPAS transmissions.

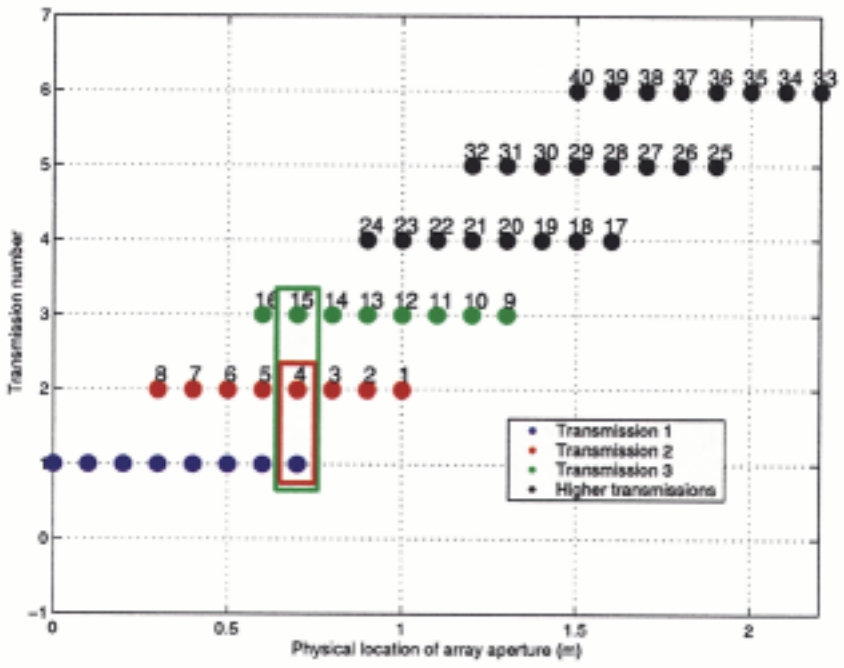

Fig. 8. The spatial elements of maximum inter-transmission correlation are determined by the speed of the AUV. Here the horizontal translation of the physical aperture is shown for three subsequent transmissions. One sees that for AUV translations of 0.3 m between TOPAS transmissions, the fourth element of the physical aperture occupys the same spatial location for the second transmission as the 1st element during the first. Similarly, the seventh element occupies the same position as the first for the third transmission. In Fig. 7 the seventh position of the perture is plotted as "Element index" 15, following the number scheme shown on this figure. Higher transmissions are uncorrelated with the first element of the first transmission because no array elements can occupy the same space due to the combination of the size of the aperture and the speed of the AUV.

height of the AUV above S3 and $y - y_o$ is the linear distance along the trajectory away from the point of closest approach. Then, if S2 is hypothesized to lie a distance $[\Delta x, \Delta y]$ away from S3 at the same value of Z (flat bottom hypothesis) and the bistatic angle between the direction vector connecting the source to S3 and the vector connecting S3 to the point of closest approach on the AUV trajectory is θ, then under the assumption that the source is in the far field the arrival time from the hypothesized location of S2 is closely approximated by

$$T_{\widehat{S2}} = \left(R - (x_o - \Delta x)\frac{\cos\theta}{c_o} + (y_o - \Delta y)\frac{\sin\theta}{c_o}\right) + \sqrt{(x_o - \Delta x)^2 + (y - y_o - \Delta y)^2 + \frac{z_o^2}{c_o}} + T_o. \quad (2)$$

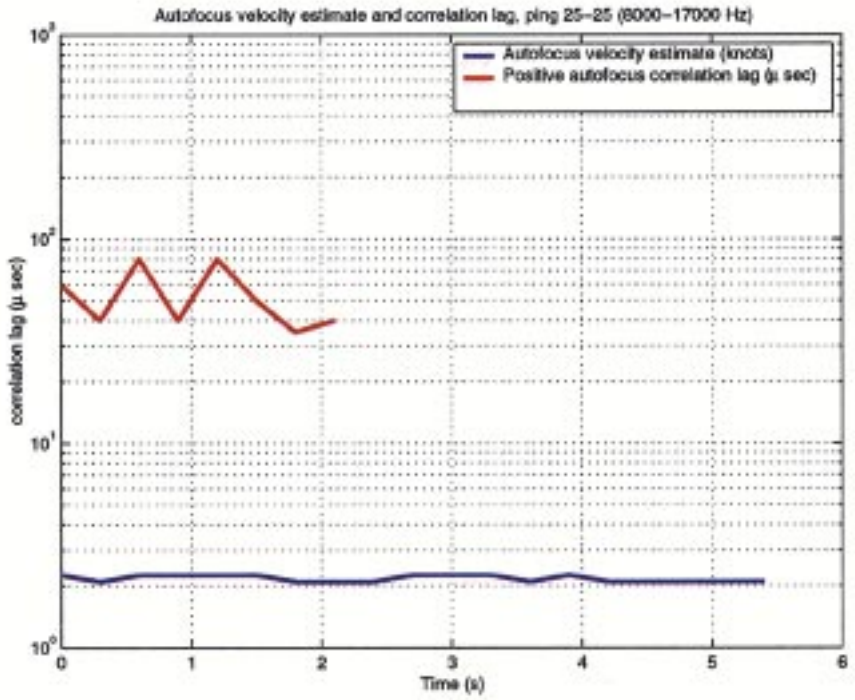

Fig. 9. The local velocity estimate from the inter-transmission correlation element lag (blue) and lag of the maximum inter-transmission correlation in time in μs (red). The estimated vehicle velocity corresponds to the known operating conditions of the AUV during ping 25 of experiment x9 814 501.

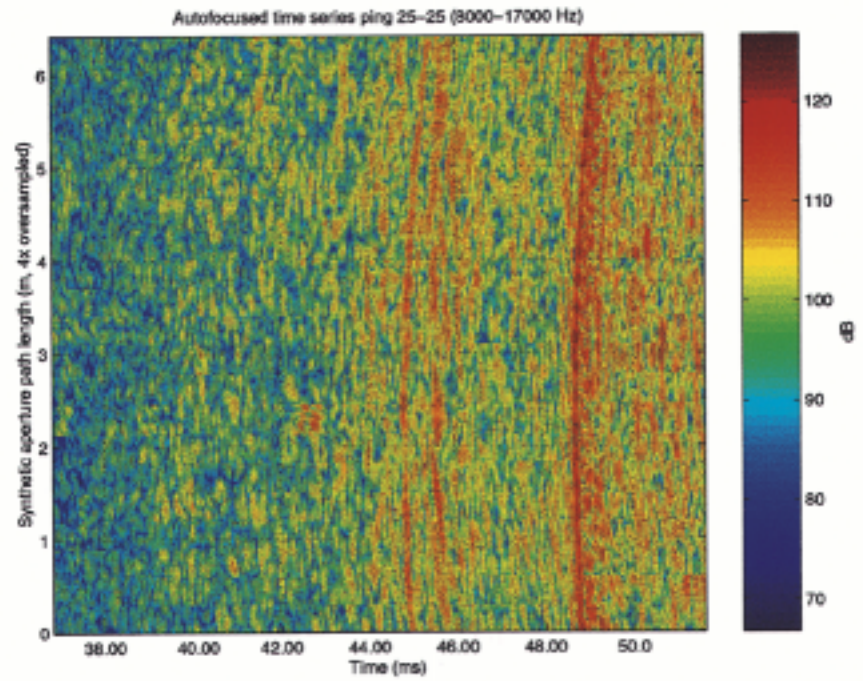

Fig. 10. The 6.3-m long synthetic aperture for ping 25 constructed by appending physical apertures at the element lag of maximum correlation, shifting the time series by the associated temporal lag of the maximum spatial lag. The resulting synthetic aperture shows that scattering from both the proud sphere S3 (times after approximately 49 ms) and the flush buried sphere S2 (two returns between 44.5 and 45.5 ms arbitrary time) has been measured in the nearfield.

A. Analysis of Subcritical Returns From S2

The result of coherently summing all the autofocused time series at the times given in (2) for a range of hypothesized values of $[\Delta x, \Delta y]$ for ping 25 from the subcritical experiment x9 814 501 is illustrated in Fig. 13. The results of the coherent summation have been envelope detected and squared and then displayed in dB. To enhance detection, the data have been filtered to the 8–17-kHz frequency band. Here it is seen that the nearfield beamformed response from S3, at a standoff range of $x_o = 8.8$ m and an along track displacement relative to the point of closest approach of $\Delta y = 0$ m, has a spatial width at the -3 dB point in the along track dimension of approximately 0.4 m, which is consistent with the theoretical resolution of a Hanning shaded 6.3 m long aperture at the estimated standoff range. The latter returns behind the first detection are assumed

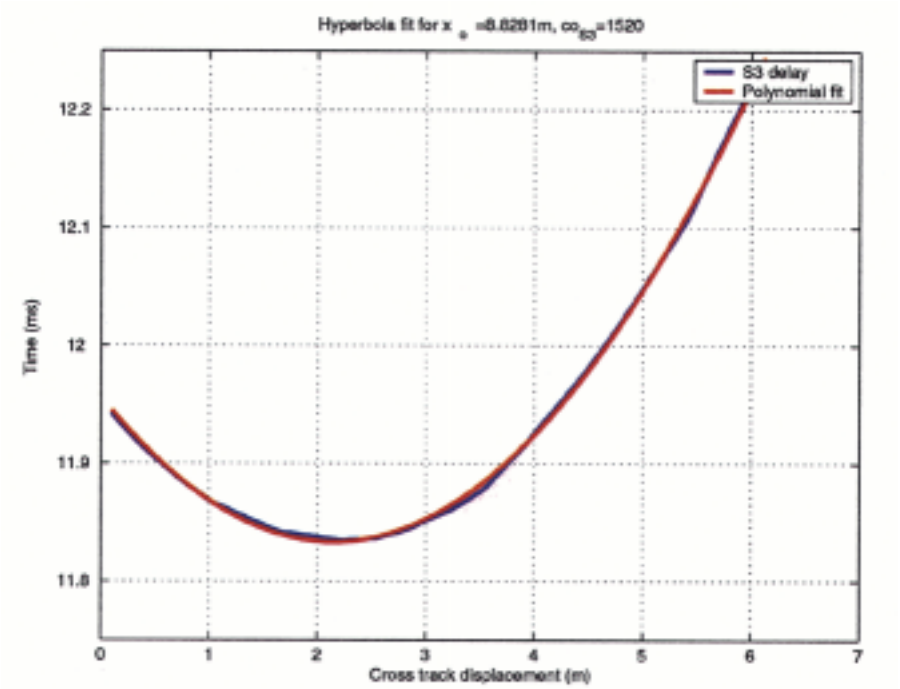

Fig. 11. The agreement between the arrival times of the scattered field from the proud sphere S3, and an analytic fit based on the assumption that the vehicle moves on a straight trajectory during ping 25 of experiment x9 814 501. The best fit was obtained with a horizontal standoff range of 8.8 m assuming a background sound speed of $c_o = 1520$ m/s.

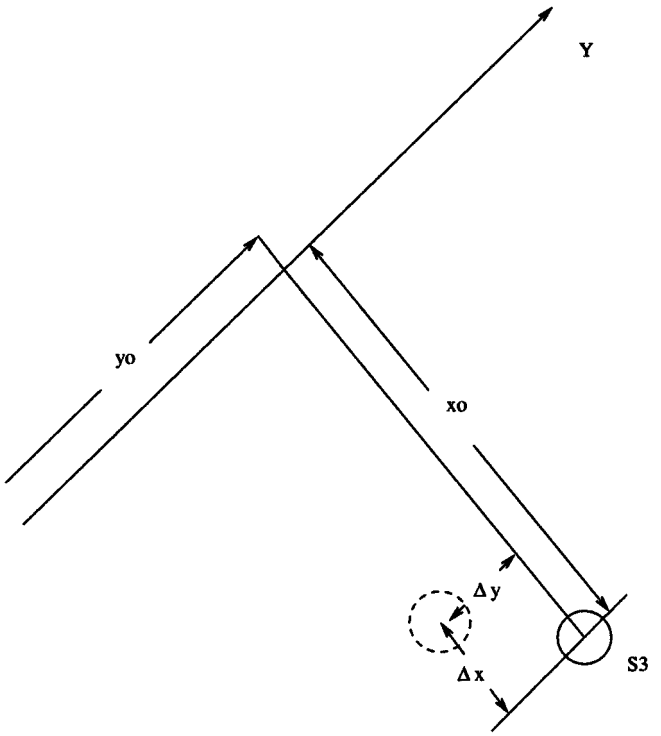

Fig. 12. The AUV trajectory notation used for determining nearfield beamforming parameters.

to be resonant returns of elastic waves in the proud sphere. Two detections of S2 are also found, at standoff ranges of approximately $\hat{x} = (x_o - \Delta x) = 5.25$ and 5.75 m and along track displacements of $y - y_o - \Delta y = -0.2$ and 1.0. The first return is hypothesized to be the first round trip of the S_o membrane wave, while the second return is hypothesized to be the first round trip of the A_{o-} antisymmetric bending wave of the target, which the modeling studies have shown arrives with a time lag of approximately 0.5 ms. The fact that the beamforming finds an along track spatial shift for this arrival is likely due to the dispersive nature of this arrival [10]. Inspection of Figs. 5, 6, and 10 shows that the delay between the first and second S2 arrivals is indeed a fairly strong function of position along the AUV trajectory and since the aperture considered here is not symmetrical about the point of closest approach, the asymmetric dispersion causes an along track shift in the beamformed results.

In Fig. 14, the hypothesized arrivals times of the first return from S2 and the S3 arrival are shown superimposed on the autofocused time series. Close inspection of the trajectories shows that they are fully coherent with the data over the entire synthetic aperture. The second S2 return is less obviously a fully coherent return over the entire synthetic aperture, consistent with modeling studies conducted at SACLANTCEN which have shown an interference structure in the sphere multipath associated with the second S_o membrane and the first A_{o-} antisymmetric wavetypes of the sphere [10].

The spectrogram of the nearfield beamformed data at the along track location of the first S2 return is illustrated in Fig. 15. The time-frequency response of S2 is found between the times of 6 and 8 ms and has a very interesting character. Between frequencies of 3 and 8 kHz, a single return is seen at a time of 6 ms, while at higher frequencies, two returns are seen at 6.5 and 7.5 ms. It is hypothesized that the lower frequency response is associated with the geometric component of the evanescent excitation and scattering from the sphere, while the first higher frequency response is associated with excitation by the evanescent lateral wave of the S_o membrane wave in the sphere at the sediment-water interface, with a subsequent return via a supercritical path. The second higher frequency return is hypothesized to be the first antisymmetric wave A_{o-}

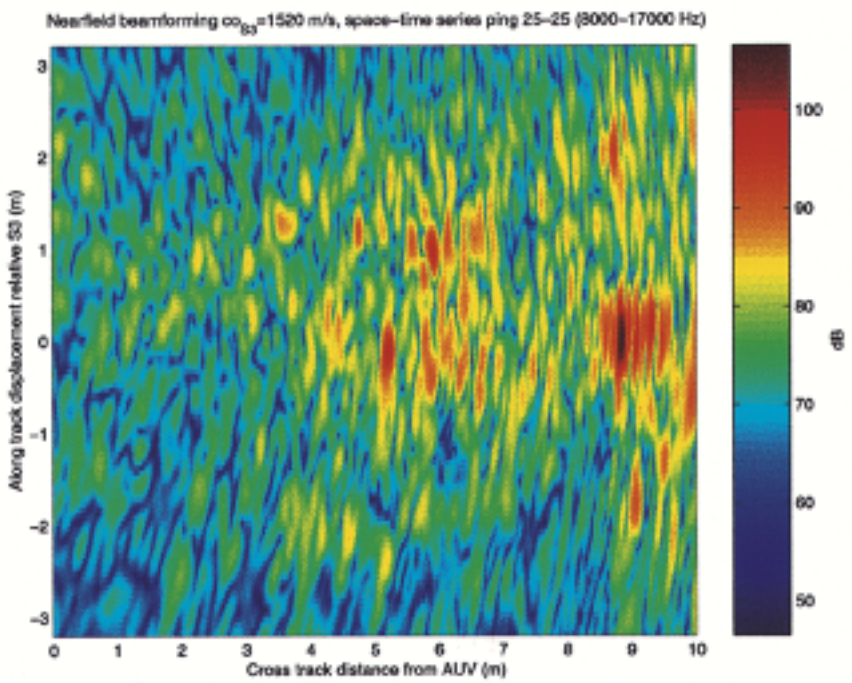

Fig. 13. The nearfield beamformed synthetic aperture for the 20 transmissions in ping 25 of experiment x9 814 501. The proud sphere is clearly seen at an along track displacement of $y - y_o = 0$ m and the cross track displacement of $x_o = 8.8$ m. Two returns from the flush buried sphere S2 are seen at standoff ranges of approximately $\hat{x} = (x_o - \Delta x) = 5.25$ and 5.75 m and along track displacements of $y - y_o = -0.2$ and 1.0. The second return is believed to be the first multipath of the A_{o-} membrane wave of the sphere.

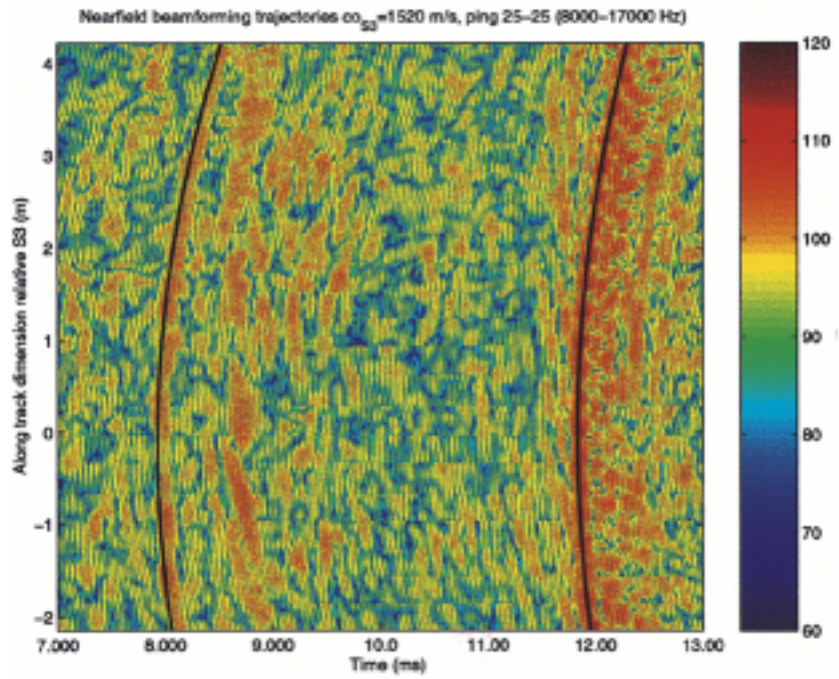

Fig. 14. Temporal trajectories corresponding to maximum returns from S2 (left curve) and S3 (right curve). Close inspection of these trajectories show that the scattered field from these two targets is being coherently summed over the entire 6.3 m synthetic aperture constructed for ping 25.

re-radiating by the same path. However, without supporting modeling studies, these results remain open to interpretation.

B. Analysis of Supercritical Returns From S2

A supercritical data set from experiment x9 814 601 has also been analyzed to show how the returns from S2 change when it is insonified at higher grazing angles. During this experiment, the TOPAS source was moved forward to a position of 12.5 m along the rail and the source was pointed at the S2 target. At this source position, the buried targets S1 and S2 are more strongly excited than in experiment x9 814 501 for three reasons, 1) because they are insonified at higher grazing angles of 24.4° (S2) and 30.5° (S1) which are both above the critical angle, 2) because the source is focused on S2 instead of S3, so S1 is inside the insonified patch and 3) because the source is only 20 m from S1, so there is less transmission loss than in experiment

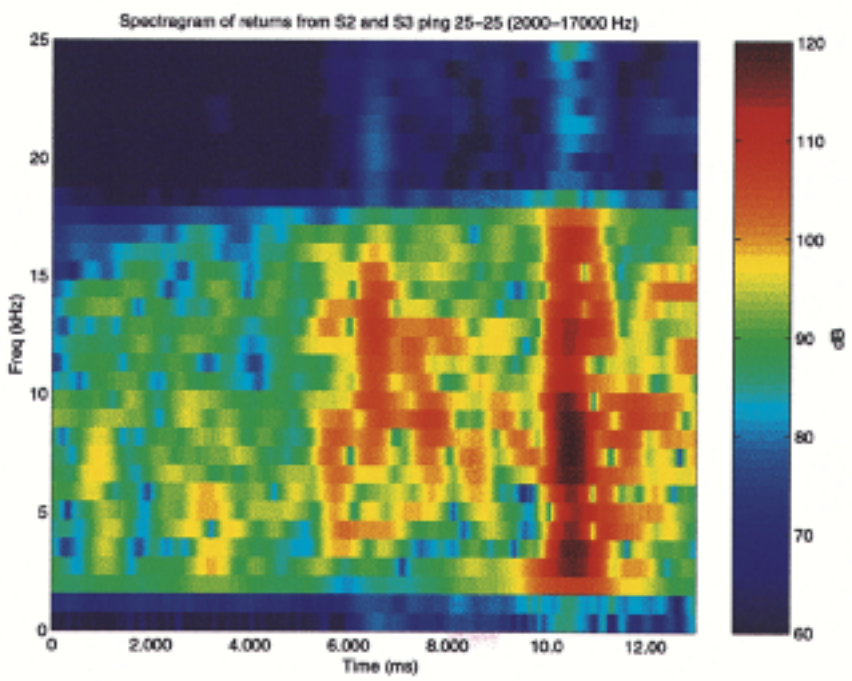

Fig. 15. The spectrogram of the beamformed time series for ping 25 centered on the image of S2. Clearly visible is the time frequency response of the flush buried sphere between times of 6 and 8 ms. Below 8 kHz, S2 has one weak return at 6 ms, while in the 8–15-kHz range there are two distinct returns, the second of which is considered to be a membrane wave multipath of the sphere. The return from the proud sphere S3 is clearly visible at 10.5 ms. The source spectrum of the incident 8-kHz Ricker has not been deconvolved from this result.

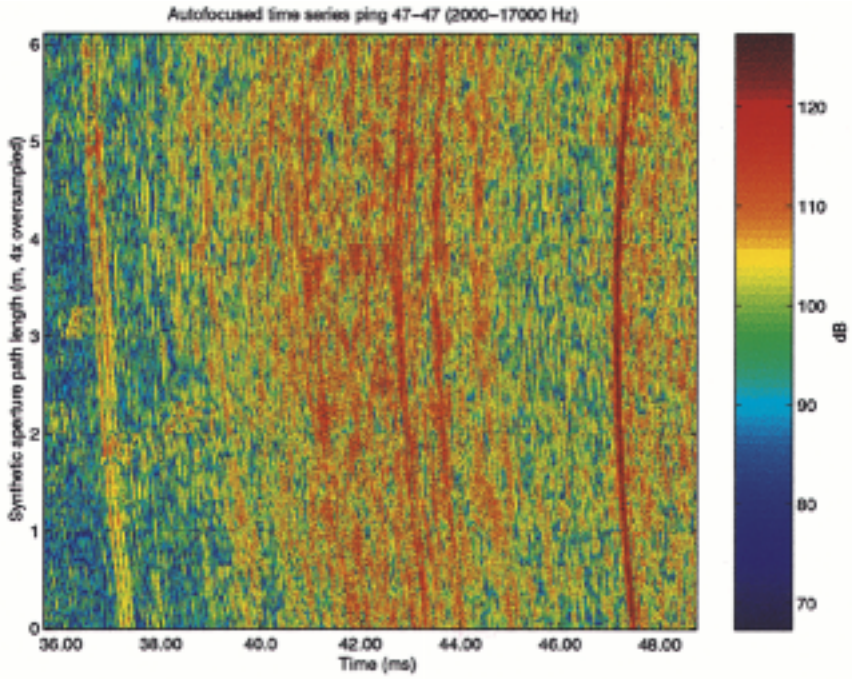

Fig. 16. The 6.1-m long synthetic aperture constructed for 18 transmissions from ping 47 of experiment x98 145 601. Here the TOPAS is focused on S2 and the AUV passes almost directly over this target at a favorable bistatic angle. The return from S1 is faintly visible between 39 and 40 ms arbitrary time. The S2 returns are visible between 42 and 44 ms and the S3 returns commence at about 47 ms.

x9814501, where the source was 7.5 m further away. In addition, the scattered returns from the rough sandy bottom are much larger for the first and third reason. The result is that the RNR increases from the 4 to 10 dB seen in experiment x9 814 501 for ping 25 to values between 8 and 15 dB for ping 47 in experiment x9 814 601. Although both the target scattering and the reverberation is increased for the supercritical experiment, the results seem to indicate that the flush buried sphere S2 becomes slightly more visible against the background reverberation, ie that the SRR is slightly increased for supercritical detection of S2.

In Fig. 16, the 6.1-m long autofocused synthetic aperture response for ping 47 of experiment x9 814 601 is shown. The return from the proud sphere S3 is seen after times of 47 ms, while the scattered return from the rough sandy sediment-water inter-

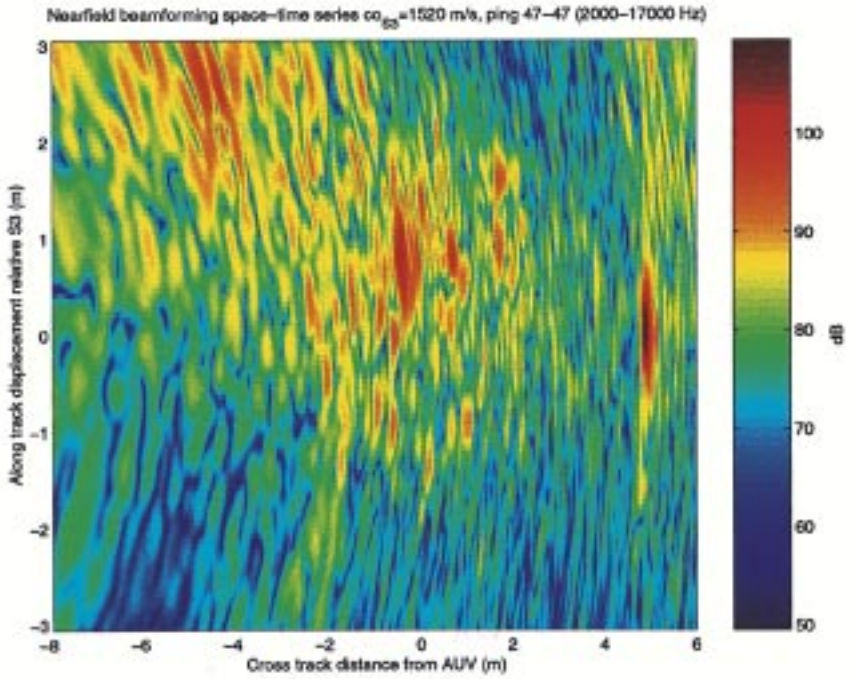

Fig. 17. The nearfield beamformed image of the target field for ping 47 from experiment x9814601, where the TOPAS is directed toward S2 at a 24.4° grazing angle. The target of opportunity is at $y - y_o = 0$ m and $x_o = 4.9$ m. The first return from S2 is at $y - y_o = 0.8$ m and $x = -0.5$ m. The faint return from S1, insonified above critical at a grazing angle of 30.5° is seen at $x = -5$ m and $y - y_o = 2.6$ m.

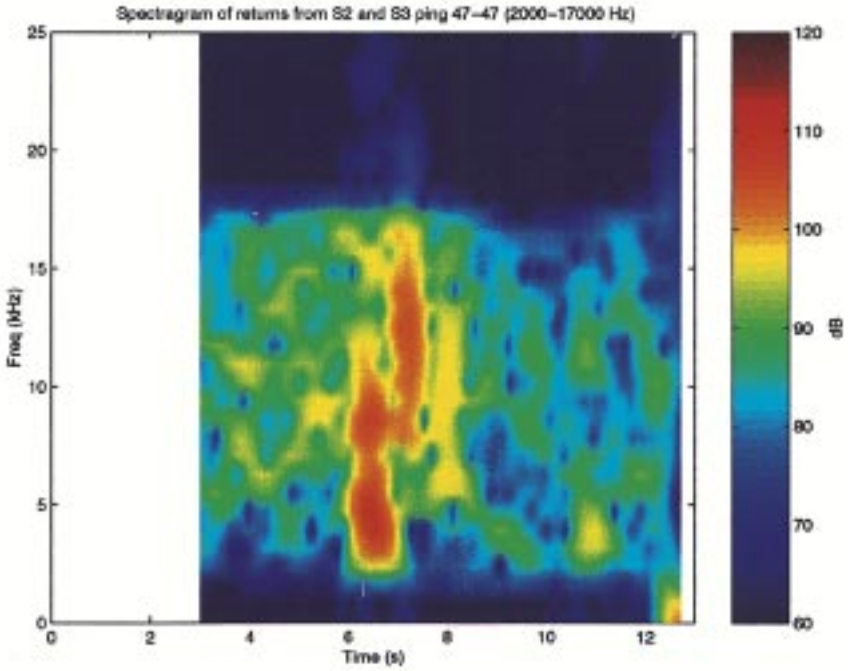

Fig. 18. The spectrogram of the beamformed time series from ping 47 from experiment x9814601, where S2 is insonified above critical at 24.4° clearly shows a stronger first arrival between 2 and 11 kHz at 6.4 ms, followed by the first multiple between 7 and 16 kHz at 7.2 ms. A second elastic multiple is seen between 5 and 13 kHz at 8 ms.

face is seen between times of 39 to 45 ms. Inside this scattering are buried the returns from S1 (between 39 and 40 ms) and S2 (between 43 and 44 ms). The strong return to the far left between 36 and 37 ms is a source multiple.

The result of nearfield beamforming Fig. 16 are shown in Fig. 17. As opposed to ping 25 from experiment x9814501, here the imaging results show that the AUV was not traversing perpendicular to the target field axis. The proud sphere S3 is imaged at $y-y_o = 0$ m, $x = 4.9$ m, the first return from S2 is imaged at $y-y_o = 0.8$ m, $x = -0.5$ m and the return from the deep buried sphere S1 is visible at $y-y_o = 2.6$ m, $x = -5$ m. S1 and S2 are both clearly imaged in this case because they are both excited and observed above the critical angle. The spectral characteristics of these returns is also significantly changed by the more favorable geometry. The spectrogram of the return from S2 is shown in Fig. 18. Comparison with Fig. 15 shows that when the

incident field is above critical, the frequency content of the first arrival, which is hypothesized to be specular in nature, extends all the way to the low frequency cutoff of the analysis band, while the second and third returns associated with the elastic response of the sphere are less strongly affected by the angle of incidence.

V. Conclusions

Results from the GOATS'98 experiment indicate that bistatic synthetic apertures may be reliably generated by AUVs for the enhanced detection of objects buried in fast sediments and insonified below the critical angle in the 2–20-kHz frequency range. Difficulties associated with inaccurate vehicle navigation and poor intra-vehicle communication can be largely overcome when the vehicle flies in a straight line and a target or transponder of opportunity is available to anchor the processing in space. Such a known target or transponder is required to determine the standoff distance of the synthetic aperture, since the actual trigger time of the bistatic source is assumed to be unknown to the AUV. One potential known target could be the closest pinger in a LBL network. In the results presented here, simple correlation autofocusing was combined with the availability of the proud target S3 to generate a nearfield time series and to beamform it as a function of cross and along track distance from the AUV trajectory to obtain images of buried objects.

Results show that when excited by an 8-kHz Ricker pulse below the critical angle of the sediment and observed bistatically above the critical angle, the flush buried sphere S2 was most visible in the 8–15-kHz frequency band, with lower levels of bistatic scattering in the 3–8-kHz band. These results conflict with the suggestion that subcritical detection of buried objects is best performed at the lowest possible frequencies, the logic of which relies on the idea that the mechanism for target insonification and subsequent rescattering is the evanescent wave, which exponentially decreases its penetration at higher frequencies. Also, in the case of this experiment, penetration due to scattering from ripples is not an important mechanism for the excitation of buried targets due to the smoothness of the sand in the target field. Instead it is hypothesized that this unexpected high frequency response of S2 is associated with excitation and re-radiation of membrane waves in the part of the target closest to the seabed. Analysis of experiment x9 815 601 also shows that when S2 is insonified above the critical angle, the low frequency response is enhanced. It is possible that in the experimental scenarios examined in this paper, where the AUV passes bistatically over the scatterers at above critical angle, the favorable reradiation of the scattered field into high angles makes the targets more visible in the higher frequency range of the 2–20-kHz band. Further processing of bistatic data collected both on the AUV and on the bistatic HLA deployed during this experiment and further modeling studies are required to determine conclusively, the mechanisms for the excitation and subsequent scattering from buried objects observed in bistatic geometries.

Acknowledgment

The authors wish to acknowledge J. Edwards, MIT, and E. Bovio and R. Hollett, SACLANTCEN for their assistance in acquiring and processing the AUV data used in this paper.

References

[1] H. Schmidt, A. Maguer, E. Bovio, W. L. J. Fox, K. LePage, N. G. Pace, R. Hollett, P. Guerrini, P. A. Sletner, E. Michelozzi, B. Moran, and R. Grieve, "Generic Oceanographic Array Technologies (GOATS)'98—Bistatic Seabed Scattering Measurements Using Autonomous Underwater Vehicles," SACLANT Undersea Research Centre, La Spezia, Italy, SR-302, 1998.

[2] L. J. Cutrona, "Comparison of sonar system performance achievable using synthetic-aperture techniques with the performance achievable by more conventional means," *J. Acoust. Soc. Amer.*, vol. 58, no. 2, pp. 336–348, 1975.

[3] A. Maguer, E. Bovio, W. L. J. Fox, and H. Schmidt, "*In situ* estimation of sediment sound speed and critical angle," *J. Acoust. Soc. Amer.*, vol. 108, no. 3, pp. 987–996, 2000.

[4] A. Maguer, W. L. J. Fox, H. Schmidt, E. Pouliquen, and E. Bovio, "Mechanisms for subcritical penetration into a sandy bottom: Experimental and modeling results," *J. Acoust. Soc. Amer.*, vol. 107, no. 3, pp. 1215–1225, 2000.

[5] O. Bergem and N. G. Pace, "Calibration of the TOPAS PS040. Part I: Measurements Recorded With the TOPAS Acquisition System," SACLANT Undersea Research Centre, La Spezia, Italy, SM-119, 1996.

[6] R. W. Sheriff, "Synthetic aperture beamforming with automatic phase compensation for high frequency sonars," in *Proc. 1992 Symp. Autonomous Underwater Vehicle Technology AUV '92*, 1992, pp. 236–245.

[7] A. Bellettini, S. Fioravanti, and M. Pinto, "Preliminary Experimental Investigation of Synthetic Aperture Sonar Micronavigation," SACLANT Undersea Research Centre, La Spezia, Italy, SM-355, 1999.

[8] M. A. Pinto, S. Fioravanti, and E. Bovio, "Accuracy of Synthetic Aperture Sonar Micronavigation Using a Displaced Phase Center Antenna," SACLANT Undersea Research Centre, La Spezia, Italy, SM-352, 1998.

[9] A. Tesei, A. Maguer, W. L. J. Fox, and H. Schmidt, "Measurements of Acoustic Scattering From Partially and Completely Buried Spherical Shells," SACLANT Undersea Research Centre, La Spezia, Italy, SM-362, 1999.

[10] M. A. Pinto, A. Bellettini, R. Hollett, and A. Tesei, "High resolution imaging of buried targets," *IEEE J. Ocean. Eng.*, pp. 484–494, July 2002.

[11] P. N. Denbigh, "A design study for a correlation log to measure speed at sea," *J. Navigation*, vol. 35, pp. 160–184, 1982.

Kevin D. LePage was born in East Lansing, MI, in 1961. He received the B.S. degree from Webb Institute of Naval Architecture, Glen Cove, NY, in 1983, and the S.M. and Ph.D. degrees in ocean engineering from Massachusetts Institute of Technology, Cambridge, in 1986 and 1992, respectively.

From 1983 to 1987, he was a Naval Architect at Dano Taylor Naval Research and Development Center (DTNSRDC), Cabin John, MD, where he developed conceptual designs for naval combatants. From 1992 to 1997, he was a Scientist and later a Senior Scientist at Bolt, Straner & Newman (BBN), Cambridge, MA, where he worked on problems related to propagation and scattering in the Arctic, hydroacoustic detection of nuclear detonations, active noise and vibration control and structural acoustics. Since 1997, he has been a Senior Scientist at SACLANT Undersea Research Centre, La Spezia, Italy, where his primary responsibility has been the development of acoustic models for the prediction of scattering and reverberation in shallow and very shallow water at low to mid frequencies.

Henrik Schmidt was born in Aabenra, Denmark in 1950. He received the M.S. degree in civil engineering and the Ph.D. degree in experimental mechanics from the Technical University of Denmark, Lyngby, Denmark in 1974, and 1978, respectively.

Holding positions of Research Fellow from 1978 to 1980 at the Technical University of Denmark, and from 1980 to 1982, at Risoe National Laboratory, Roskilde, Denmark, he worked on numerical modeling of wave propagation and scattering phenomena in relation to nondestructive testing of structures. From 1982 to 1987, he was Scientist and Senior Scientist at the SACLANT Undersea Research Centre, La Spezia, Italy, where he developed the SAFARI code for modeling seismo-acoustic propagation in ocean waveguides. In 1987, he joined Massachusetts Institute of Technology, Cambridge, where he is currently a Professor and Associate Head of Ocean Engineering. His primary research interest is the interaction of underwater sound with seismic waves in the seabed and the Arctic ice cover. Other interests include computational acoustics and matched field processing and the use of acoustics in autonomous oceanographic sampling networks.

Prof. Schmidt is a Fellow of the Acoustical Society of America and a member of the Society of Exploration Geophysicists.